Journal of Photochemistry and Photobiology A: Chemistry 241 (2012) 26–37

Contents lists available at SciVerse ScienceDirect

Journal of Photochemistry and Photobiology A: Chemistry

journal homepage: www.elsevier.com/locate/jphotochem

Synthesis, characterization and optical properties of aryl and diaryl substituted phenanthroimidazoles

Manoj Kumar Nayak*

Department of Chemistry, Texas A&M University at Qatar, Qatar Foundation, PO Box 23874, Doha, Qatar

ARTICLE INFO

Article history:
Received 14 January 2012
Received in revised form 8 May 2012
Accepted 18 May 2012
Available online 29 May 2012

Keywords:
Phenanthroimidazoles
Excited state intramolecular proton transfer (ESIPT)
Photoluminescence
Restricted intramolecular rotation
Intramolecular charge transfer (ICT)
Density functional theory (DFT)

ABSTRACT

This article presents a facile synthesis of novel class of blue-green fluorescent phenanthroimidazoles and report on their optical, electrochemical, and thermal properties. Detailed photophysical and quantum chemical studies with a series of hydroxy-, methoxy-, nitro-, amino- and tosylaminophenyl substituted derivatives of 2-phenyl-1*H*-phenanthro[9,10-*d*]imidazole and 1,2-diphenyl-1*H*-phenanthro[9,10-*d*]imidazole have been performed to elucidate the origin of the surprisingly divergent emission shifts. Out of these, three dyes (HPhI, HPPhI, and TsPPhI) undergo excited state intramolecular proton transfer (ESIPT) reaction leading a large Stokes' shifted fluorescence emission from the phototautomer. The results of quantum chemical investigations not only confirmed the intramolecular charge transfer characteristics of the ESIPT tautomers but also provided a rational for the observed high fluorescence quantum efficiency in the solid state. The high photoluminescence quantum yield ($\Phi^{PL} \sim 39$–68%) in the solid state is ascribed to twisted chromophores due to phenyl substituents at 1,2-position of the phenanthroimidazole ring which restricted intramolecular motion, leading to an optically allowed lowest optical transition without self quenching.

1. Introduction

Proton- and charge-transfer reactions are most fundamental processes involved in chemical reactions as well as in living systems [1,2]. Among the various studies of proton transfer, organic molecules exhibiting excited-state intramolecular proton transfer (ESIPT) have attracted considerable research interest from the viewpoint of the development of new functional materials for optoelectronic applications such as UV photostabilizers [3], photoswitches [4], fluorescent probes [5], and organic light-emitting diodes (OLEDs) [6]. Photoinduced ESIPT is generally observed for organic compounds featuring both a protic acid group (*e.g.*, —OH, —NH_2, —$NHSO_2R$, *etc.*) and a basic site (=N—,)C=O, *etc.*) with a suitable conformation, one that forms an intramolecular hydrogen bond within the distance of 2.0 Å. For an efficient ESIPT, the acidity and/or basicity of these groups must increase upon photoexcitation [7]. Among such molecules, hydroxyphenylbenzazoles (HBA) such as 2-(2′-hydroxyphenyl)benzimidazole (HBI) [8–10], 2-(2′-hydroxyphenyl)benzoxazole (HBO) [10–12], 2-(2′-hydroxyphenyl)benzthiazole (HBT) [10,13], 2-(2′-arylsulfonamidophenyl)benzimidazole [14,15] and 2-(2′-arylsulfonamidophenyl)benzoxazole [16] have attracted particular attention due to their potential for fluorescent probes [17] (for the labeling of proteins and DNA) and model base pairs [18] (for studying the environments within the major and minor grooves of DNA duplexes).

The most stable form of the mentioned ESIPT molecules in the ground state is in equilibrium between several different conformers arising from tautomerism and rotamerism (Fig. 1) [8]. The normal planar *syn* form (N_{syn}) features an intramolecular hydrogen bond between protic acid group (the acidic hydroxyl or amine group) and the basic nitrogen atom of the imidazole ring. The N_{syn} conformer can undergo proton transfer to form its tautomer (T_{syn}). Upon excitation of the normal form to its first excited singlet state (N_{syn}*), undergoes an ultrafast excited-state intramolecular proton transfer to yield the planer tautomer T_{syn}* accompanied with large Stokes' shifted fluorescence emission. The *syn*-conformers can rotamerize to form their non-planar *anti* forms (N_{anti} and T_{anti}, respectively). In a protic solvent, the N_{anti} conformer can form *intermolecular* hydrogen bonds with solvent molecules, but it cannot undergo ESIPT. Therefore, dual fluorescence is frequently observed in polar protic solvents; in addition to the fluorescence from the T_{syn}* form, the N_{anti}* form can also exhibit rather normal Stokes' shifted weak fluorescence [16,19]. Moreover, the typical ESIPT process produces the tautomeric form can be coupled with the intramolecular charge transfer (ICT) state with a rotation around interannular bond to produce a non-planar configuration (T_{ICT}*) between the two rings. The T_{ICT}* state can be deactivated back to its ground state *via* radiationless relaxation.

* Tel.: +974 4423 0380; fax: +974 4423 0060.
E-mail addresses: manoj.nayak@qatar.tamu.edu, manoj17675@yahoo.com

1010-6030/$ – see front matter © 2012 Elsevier B.V. All rights reserved.
http://dx.doi.org/10.1016/j.jphotochem.2012.05.018

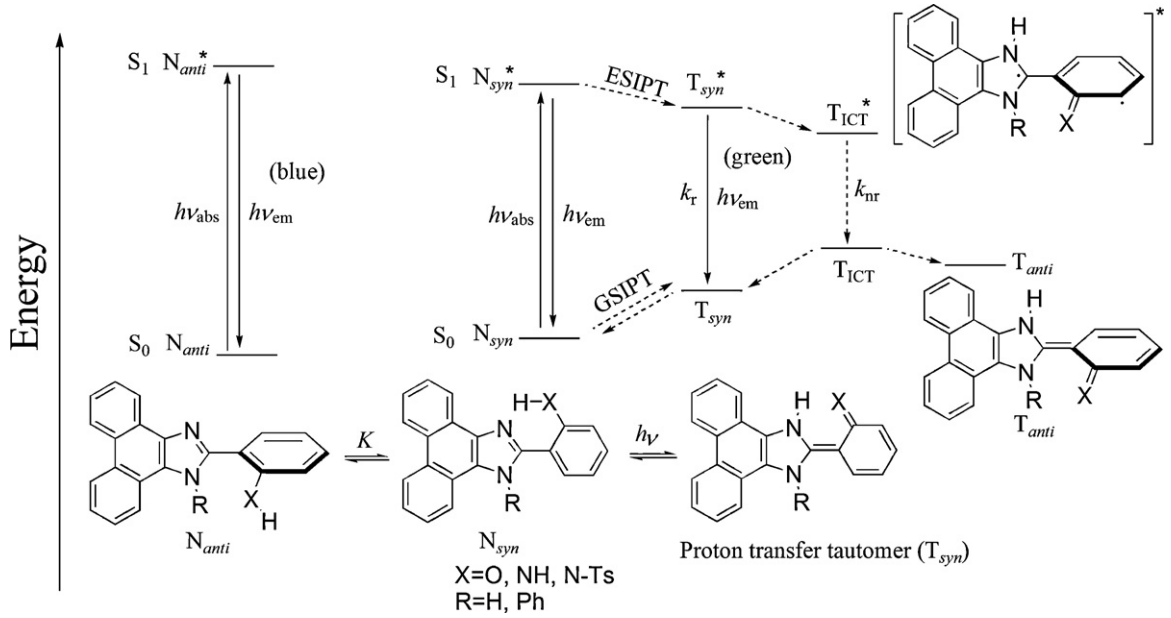

Fig. 1. Structures of various isomers of phenanthroimidazole derivatives in the ESIPT and ICT processes. From the TD-DFT results, the *o*-quinoid structures are presented for the tautomeric and ICT forms.

The ESIPT molecules exhibit rather low fluorescence quantum efficiency in the solid state due to concentration quenching, deactivation by various pre-existing isomers, and the ICT states. Aiming at the high performance OLEDs as well as the solid-state lasers, a high value of solid-state fluorescence quantum efficiency with understanding and control of radiative and non-radiative decay processes is basically in demand to contribute to the improvement of their technological applications [20,21]. Recently, a number of papers have been published reporting conjugated organic small molecules that showed high quantum yield in the solid state without concentration quenching problem [22–28]. In solution, the conjugated backbone of these molecules is significantly twisted by steric hindrance [23] and the radiative decay pathway of the resulting twisted chromophores [24] is generally suppressed as they dissipate energy for molecular rotation. In the solid state, the twisted conjugated backbone, however, enhances the emissive property of the molecules because the molecular rotation is hindered by adjacent molecules upon aggregation [23–28].

A rational design to maximize the ESIPT signal demands new strategies to minimize the content of N_{anti} and T_{anti}, while preserving the valuable optical characteristics of HBA. With this intention, described herein is the synthesis of *o*-substituted 2-phenyl-1*H*-phenanthro[9,10-*d*]imidazole (PhI) and 1,2-diphenyl-1*H*-phenanthro[9,10-*d*]imidazole (PPhI) derivatives and the substituent effects on their ESIPT processes, rotational processes, and optical properties. To elucidate the higher fluorescence quantum efficiencies of 2-(1*H*-phenanthro[9,10-*d*]imidazol-2-yl)phenol (HPhI), 2-(1-phenyl-1*H*-phenanthro[9,10-*d*]imidazol-2-yl)phenol (HPPhI) and 4-methyl-*N*-(2-(1-phenyl-1*H*-phenanthro[9,10-*d*]imidazol-2-yl)phenyl)benzenesulfonamide (TsPPhI) in the solid state than those in solution, structural analyses and time-dependent density functional theory (TD-DFT) calculations were carried out, which was correlated with their photophysical properties. The model compounds 2-(2-methoxyphenyl)-1*H*-phenanthro[9,10-*d*]imidazole (MPhI), 2-(2-methoxyphenyl)-1-phenyl-1*H*-phenanthro[9,10-*d*]imidazole (MPPhI), 2-(2-nitrophenyl)-1-phenyl-1*H*-phenanthro[9,10-*d*]imidazole (NPPhI), 2-(1-phenyl-1*H*-phenanthro[9,10-*d*]imidazol-2-yl)aniline (APPhI), unable to undergo ESIPT, were also studied for comparison. The results gained from this study should provide guidelines for tuning the emission properties of this class of ESIPT fluorophores with potential applications in chemistry (*e.g.*, molecular materials, probes, sensors, and tracers) and material science (*e.g.*, optoelectronics).

2. Experimental

2.1. General

All solvents and reagents were purchased from commercial sources and used as received. The column chromatography was performed with 200–400 mesh silica gel as stationary phase. The ^{1}H NMR and ^{13}C NMR (proton-decoupled) spectra were measured by using a 500 MHz instrument in $CDCl_3$ containing 0.03 (v/v)% tetramethylsilane (TMS) as the internal standard (^{1}H NMR: TMS at 0.00 ppm, $CDCl_3$ at 7.24 ppm, and ^{13}C NMR: $CDCl_3$ at 77.23 ppm). Proton coupling patterns were described as singlet (s), doublet (d), triplet (t), quartet (q), multiplet (m) and broad (br). Coupling constants (*J*) are quoted in Hertz (Hz). Mass Spectra were recorded on a mass spectrometer by the electron impact (EI) ionization technique. The thermal properties of the materials were examined by differential scanning calorimetry (DSC) at heating rate of 10 °C min^{-1} under N_2. UV–visible absorption and corrected fluorescence spectra (with excitation wavelengths of λ_{exc} = 325 or 355 nm) were recorded in argon-bubbled $CHCl_3$, CH_3CN and 1-propanol, respectively at room temperature with a fixed emission and excitation slit width of 2 nm each. The fluorescence quantum yields (Φ^{PL}) were determined in different solvents at 298 K against the 9,10-diphenylanthracene standard (Φ^{PL} = 0.84) in benzene [29]. On the other hand, Φ^{PL} of PMMA film doped with 5 wt% of aryl phenanthroimidazole dyes on the wedged quartz plate were measured using a 6-in. integrating sphere equipped with a 325-nm CW He-Cd laser and a PMT detector attached to a monochromator. The detailed analytical procedure to obtain solid-state Φ_{PL} has been described elsewhere [30]. Cyclic voltammetric experiments were carried out using three-electrode cell assemblies including a glassy-carbon working electrode, a platinum wire counter electrode, and a Ag/Ag$^+$ reference electrode. After argon saturation in one compartment cell, measurements were carried

out in dichloromethane (DCM) solution with tetrabutylammonium tetrafluoroborate (Bu_4NBF_4) as a supporting electrolyte at a scan rate of 100 mV s^{-1}. Each potential was calibrated with ferrocene as a reference [31].

2.2. Synthesis of phenanthroimidazoles

2.2.1. 2-(1H-Phenanthro[9,10-d]imidazol-2-yl)phenol (HPhI)

A solution of phenanthrene-9,10-dione (2.04 g, 9.82 mmol), salicylaldehyde (1.2 g, 9.82 mmol) and ammonium acetate (5.67 g, 73.55 mmol) in glacial acetic acid (40 mL) was refluxed under nitrogen for 4 h, during which time a brownish yellow precipitate formed. An excess of de-ionized water (30 mL) was added to complete the precipitation. The crude product was collected by filtration, washed with water, dried by suction. The resultant solid was dissolved in the minimum volume of DCM and purified by flash chromatography on a silica gel column using eluent 25–30 (v/v)% of ethyl acetate in *n*-hexane to give 1.62 g (5.22 mmol, 53% yield) of pure product HPhI as a white solid. m.p. 260 °C; ^{1}H NMR ($CDCl_3$, 500 MHz), δ = 11.53 (s, 1H), 8.74 (t, *J* = 9.51, 8.95 Hz, 2H), 8.51 (d, *J* = 7.37, 1H) 8.34 (d, *J* = 7.27 Hz, 1H), 8.16 (d, *J* = 7.83 Hz, 1H), 7.73 (m, 4H), 7.44 (t, *J* = 7.98, 7.47 Hz, 1H), 7.17 (d, *J* = 8.39 Hz, 1H), 7.06 ppm (t, *J* = 7.53 Hz, 1H); ^{13}C NMR ($CDCl_3$, 125 MHz) δ = 162.08, 158.31, 143.63, 133.68, 133.24, 129.63, 129.27, 127.84, 127.71, 126.97, 126.88, 126.73, 125.35, 124.03, 123.75, 123.08, 121.10, 120.91, 119.89, 117.68, 111.33 ppm; MS (EI) *m*/*z* 310 (M^+, 100.0), 282 (7.7), 254 (6.4), 221 (3.3), 164 (14.2), 127 (5.0), 74 (1.6); HRMS calcd for $C_{21}H_{14}N_2O$: 310.11, found: 310.09; Element analysis calcd (%) for $C_{21}H_{14}N_2O$: C 81.27, H 4.55, N 9.03, and O 5.16; found: C 80.76, H 4.49, N 8.81, and O 5.32.

2.2.2. 2-(2-Methoxyphenyl)-1H-phenanthro[9,10-d]imidazole (MPhI)

Compound HPhI (0.25 g, 0.80 mmol) was dissolved in DMF (5 mL) at room temperature. K_2CO_3 (0.12 g, 0.86 mmol) and MeI (0.17 g, 1.19 mmol) was added dropwise to this solution. The reaction mixture was stirred under dark conditions for 20 h. Water (20 mL) was added to the reaction mixture and extracted using ethyl acetate (50 mL × 2). The organic layer was washed with water (20 mL), brine (20 mL), and dried over $MgSO_4$. The solvent was evaporated under reduced pressure and the product obtained was purified on a silica gel column using eluent 10–15 (v/v)% of ethyl acetate in *n*-hexane to give 0.25 g (0.77 mmol, 94% yield) of pure product MPhI as a white solid. m.p. = 158 °C; ^{1}H NMR ($CDCl_3$, 500 MHz) δ = 8.75 (d, *J* = 8.43 Hz, 1H), 8.73 (d, *J* = 8.45 Hz, 1H), 8.67 (dd, *J* = 8.03 1H), 8.34 (dd, *J* = 7.42, 7.80 Hz, 1H), 8.26 (dd, *J* = 7.71 Hz, 1H), 7.69 (m, 4H), 7.50 (t, *J* = 7.38, 8.42 Hz, 1H), 7.15 (t, *J* = 7.57 Hz, 1H), 7.12 (d, *J* = 8.40 Hz, 1H), 4.06 ppm (s, 3H); ^{13}C NMR ($CDCl_3$, 125 MHz) δ = 161.08, 158.41, 144.90, 135.56, 132.52, 131.34, 129.51, 129.08, 127.55, 127.41, 126.54, 126.50, 126.23, 123.95, 123.60, 123.39, 121.39, 121.25, 121.05, 116.95, 112.43, 56.45 ppm; MS (EI) *m*/*z* 324 (M^+, 100.0), 296 (22.0), 282 (10.0), 253 (3.4), 194 (5.0), 179 (5.7), 163 (15.8), 133 (4.1), 118 (25.9), 91 (1.6); HRMS calculated for $C_{22}H_{16}N_2O$: 324.13, found: 324.11; Elemental analysis calcd (%) for $C_{22}H_{16}N_2O$: C 81.46, H 4.97, N 8.64, and O 4.93; Found: C 81.12, H 4.97, N 8.55, and O 5.18.

2.2.3. 2-(1-Phenyl-1H-phenanthro[9,10-d]imidazol-2-yl)phenol (HPPhI)

A mixture of salicylaldehyde (1.2 g, 9.82 mmol) and phenanthrene-9,10-dione (2.04 g, 9.82 mmol) were dissolved in glacial acetic acid (40 mL) at room temperature. Aniline (1.37 g, 14.7 mmol) was added dropwise to the above solution; subsequently ammonium acetate (3.9 g, 49 mmol) was added to it. The mixture was heated to reflux at 110 °C for 20 h, during which time a yellow precipitate formed. An excess of de-ionised water (30 mL) was added to complete the precipitation. The crude product was collected by filtration, washed with water, dried by suction. The resultant solid was dissolved in the minimum volume of DCM and purified by flash chromatography on a silica gel column using eluent 20–25 (v/v)% of ethyl acetate in *n*-hexane to give 2.28 g (5.90 mmol, 60.0% yield) of pure product HPPhI as an off white solid. m.p. 184 °C; ^{1}H NMR ($CDCl_3$, 500 MHz), δ = 13.83 (s, 1H), 8.75 (d, *J* = 8.38 Hz, 1H), 8.70 (d, *J* = 4.23, 1H), 8.68 (d, *J* = 4.54 Hz, 1H), 7.76 (m, 4H), 7.67 (t, *J* = 7.71, 7.39 Hz, 1H), 7.61 (d, *J* = 7.52 Hz, 2H), 7.51 (t, *J* = 8.04, 7.64 Hz, 1H), 7.24 (t, *J* = 7.79, 7.30 Hz, 1H), 7.21 (t, *J* = 7.53 Hz, 1H), 7.12 (d, *J* = 7.99 Hz, 1H), 7.03 (d, *J* = 8.36 Hz, 1H), 6.72 (d, *J* = 8.18 Hz, 1H), 6.49 ppm (t, *J* = 7.62, 7.35 Hz, 1H); ^{13}C NMR ($CDCl_3$, 125 MHz) δ = 159.46, 148.68, 139.31, 134.67, 131.11 (2C), 130.94, 130.85, 129.72, 129.32 (2C), 128.67, 127.73, 127.27, 126.75, 126.29 (2C), 126.04, 125.48, 124.41, 123.43, 122.85, 122.82, 121.10, 118.28, 118.26, 113.34 ppm; MS (EI) *m*/*z* 386 (M^+, 100.0), 369 (6.3), 357 (3.1), 281 (2.2), 266 (7.0), 239 (1.7), 193 (2.2), 165 (4.1), 149 (1.2), 97 (1.7); HRMS calcd for $C_{27}H_{18}N_2O$: 386.14, found: 386.14; Element analysis calcd (%) for $C_{27}H_{18}N_2O$: C 83.92, H 4.69, N 7.25, and O 4.14; found: C 83.46, H 4.88, N 7.19, and O 4.33.

2.2.4. 2-(2-Methoxyphenyl)-1-phenyl-1H-phenanthro[9,10-d]imidazole (MPPhI)

Compound HPPhI (0.25 g, 0.65 mmol) was dissolved in DMF (5 mL) at room temperature. K_2CO_3 (0.10 g, 0.73 mmol) and MeI (0.14 g, 0.98 mmol) were added to this solution. The reaction mixture was stirred under dark conditions for 20 h. Water (20 mL) was added to the reaction mixture and extracted using ethyl acetate (60 mL × 2). The organic layer was washed with water (50 mL), brine (50 mL), and dried over $MgSO_4$. The solvent was evaporated under reduced pressure and the product obtained was purified on a silica gel column using eluent 10–15 (v/v)% of ethyl acetate in *n*-hexane to give 0.21 g (0.52 mmol, 81% yield) of pure product MPPhI as a white solid. m.p. 211 °C; ^{1}H NMR ($CDCl_3$, 500 MHz), δ = 8.84 (d, *J* = 8.13 Hz, 1H), 8.76 (d, *J* = 8.36 Hz, 1H), 8.70 (d, *J* = 8.35 Hz, 1H), 7.70 (t, *J* = 7.01, 7.79 Hz, 1H), 7.61 (t, *J* = 7.73 Hz, 1H), 7.49 (m, 2H), 7.40 (m, 5H), 7.31 (t, *J* = 7.87 Hz, 1H), 7.25 (m, 2H), 6.96 (t, *J* = 7.45 Hz, 1H), 6.72 (d, *J* = 8.38 Hz, 1H), 3.53 ppm (s, 3H); ^{13}C NMR ($CDCl_3$, 125 MHz) δ = 157.90, 150.20, 138.59, 137.78, 132.77, 131.34, 129.41, 129.17 (3C), 128.80 (2C), 128.40, 127.69, 127.64, 127.39, 126.33, 125.57, 124.96, 124.28, 123.33, 123.27, 123.12, 121.23, 120.58, 110.75, 55.15 ppm; MS (EI) *m*/*z* 400 (M^+, 100.0), 382 (57.9), 369 (31.3), 355 (4.8), 323 (3.6), 295 (11.6), 267 (4.3), 239 (2.1), 219 (7.6), 200 (10.0), 183 (8.9), 165 (6.7), 132 (1.2), 77 (1.1); HRMS calcd for $C_{28}H_{20}N_2O$: 400.16, found: 400.16; Element analysis calcd (%) for $C_{28}H_{20}N_2O$: C 83.98, H 5.03, N 7.00, and O 4.00; found: C 83.44, H 5.08, N 6.89, and O 4.16.

2.2.5. 2-(2-Nitrophenyl)-1-phenyl-1H-phenanthro[9,10-d]imidazole (NPPhI)

A mixture of 2-nitro-benzaldehyde (2.0 g, 13.23 mmol) and phenanthrene-9,10-dione (2.75 g, 13.20 mmol) were dissolved in glacial acetic acid (60 mL) at room temperature. Aniline (1.85 g, 19.86 mmol) was added dropwise to this solution; subsequently ammonium acetate (5.09 g, 66.03 mmol) was added to it. The mixture was heated to reflux at 110 °C for 24 h, during which time a yellow precipitate formed. An excess of de-ionized water (50 mL) was added to complete the precipitation. The crude product was collected by filtration, washed with water, dried by suction. The resultant solid was dissolved in the minimum volume of DCM and purified by flash chromatography on a silica gel column using eluent 30–35 (v/v)% of ethyl acetate in *n*-hexane to give 5.20 g (12.51 mmol, 95% yield) of pure product NPPhI as a white solid. ^{1}H NMR ($CDCl_3$, 500 MHz), δ = 8.77 (dd, *J* = 8.48 Hz, 1H), 8.75 (dd,

J = 7.54 Hz, 1H), 8.71 (dd, J = 8.62 Hz, 1H), 8.0 (d, J = 7.52 Hz, 1H), 7.7 (t, J = 7.72 Hz, 1H), 7.63 (m, 3H), 7.53 (m, 2H), 7.46 (m, 3H), 7.41 (m, 2H), 7.27 (t, J = 7.51 Hz, 1H), 7.20 ppm (d, J = 7.47 Hz, 1H); ^{13}C NMR ($CDCl_3$, 125 MHz) δ = 149.18, 147.77, 137.88, 137.46, 133.71, 133.12, 130.67, 130.08 (2C), 129.86, 129.64, 128.84 (2C), 128.55, 127.89, 127.56, 127.38, 126.87, 126.54, 125.92, 125.40, 124.84, 124.36, 123.35, 123.04, 122.97, 121.14 ppm; MS (EI) m/z 415 (M^+, 53.6), 385 (49.3), 281 (100.0), 256 (19.3), 213 (7.4), 185 (11.4), 149 (12.8), 129 (19.2), 97(19.2), 81 (33.3); HRMS calcd for $C_{27}H_{17}N_3O_2$: 415.44, found: 415.13; Element analysis calcd (%) for $C_{27}H_{17}N_3O_2$: C 78.06, H 4.12, N 10.11, and O 7.70; found: C 77.90, H 4.11, N 10.05, and O 7.94.

2.2.6. 2-(1-Phenyl-1H-phenanthro[9,10-d]imidazol-2-yl)aniline (APPhI)

A solution of NPPhI (4.5 g, 10.83 mmol) in THF and ethyl acetate mixture (200 mL) was hydrogenated at room temperature under ambient pressure in the presence of Pd on activated carbon (10 wt%, 0.75 g) as catalyst. Upon completion of the reaction (TLC), the catalyst was filtered off through a pad of celite, and the filtrate was concentrated under reduced pressure providing 4.01 g (10.4 mmol, 96% yield) of amine APPhI as a white solid. m.p. 227 °C; ^{1}H NMR ($CDCl_3$, 500 MHz), δ = 8.79 (d, J = 7.98 Hz, 1H), 8.76 (d, J = 8.29 Hz, 1H), 8.70 (d, J = 8.26 Hz, 1H), 7.72 (t, J = 7.46 Hz, 1H), 7.64 (t, J = 8.21 Hz, 1H), 7.56 (m, 3H), 7.50 (m, 3H), 7.25 (t, J = 8.21 Hz, 1H), 7.20 (d, J = 8.31 Hz, 1H), 7.04 (t, J = 8.23 Hz, 1H), 6.83 (d, J = 7.74 Hz, 1H), 6.76 (d, J = 8.09 Hz, 1H), 6.40 (t, J = 7.59 Hz, 1H), 5.31 ppm (s, 2H); ^{13}C NMR ($CDCl_3$, 125 MHz) δ = 149.78, 147.57, 139.02, 137.07, 130.50, 130.17 (2C), 130.11, 129.76, 129.46, 129.34 (2C), 128.51, 127.44, 127.30, 126.50, 125.78, 125.06, 124.32, 123.37, 123.25, 122.86, 121.30, 116.90, 116.57, 114.10 ppm; MS (EI) m/z 385 (M^+, 100.0), 369 (15.0), 266 (4.5), 192 (121), 165 (5.9), 129 (3.5), 112 (1.2), 57 (1.2); HRMS calcd for $C_{27}H_{19}N_3$: 385.16, found: 385.16; Element analysis calcd (%) for $C_{27}H_{19}N_3$: C 84.13, H 4.97, and N 10.90; found: C 83.95, H 5.02, and N 10.84.

2.2.7. 4-Methyl-N-(2-(1-phenyl-1H-phenanthro[9,10-d]imidazol-2yl)phenyl)benzenesulfonamide (TsPPhI)

To a solution of amine APPhI (1.0 g, 2.59 mmol) in anhydrous pyridine (20 mL) was added p-toluenesulfonyl chloride (0.495 g, 2.59 mmol). After stirring at room temperature for 12 h, the reaction mixture was poured into aqueous 1 M HCl (50 mL), and the product was extracted with ethyl acetate (3 × 100 mL). The organic layer was washed with brine (100 mL), dried with anhydrous $MgSO_4$, filtered, and concentrated under reduced pressure. The crude product was purified on silica gel column using eluent 30–40 (v/v)% of ethyl acetate in n-hexane to give 1.19 g (2.20 mmol, 85% yield) of pure product TsPPhI as a white solid. m.p. 266 °C; ^{1}H NMR ($CDCl_3$, 500 MHz), δ = 11.57 (s, 1H), 8.83 (d, J = 7.93 Hz, 1H), 8.80 (d, J = 8.40 Hz, 1H), 8.73 (d, J = 8.36 Hz, 1H), 7.81 (t, J = 6.93, 7.75 Hz, 2H), 7.72 (t, J = 7.72, 7.07 Hz, 1H), 7.57 (m, 2H), 7.49 (t, J = 7.76 Hz, 2H), 7.36 (d, J = 8.26 Hz, 2H), 7.25 (t, J = 7.74 Hz, 2H), 7.02 (d, J = 8.27 Hz, 1H), 6.90 (d, J = 7.98 Hz, 2H), 6.75 (m, 3H), 6.67 (d, J = 8.78 Hz, 1H), 2.03 ppm (s, 3H); ^{13}C NMR ($CDCl_3$, 125 MHz) δ = 147.08, 143.29, 138.39, 137.29, 136.52, 130.39 (2C), 130.19, 130.03, 129.90, 129.28 (2C), 129.01, 128.90 (2C), 128.68, 128.16, 127.39, 127.29 (2C), 126.68, 126.63, 126.48, 125.65, 124.85, 124.53, 124.07, 123.41, 122.95, 122.81, 121.22, 120.32, 21.31 ppm; MS (EI) m/z 539 (M^+, 100.0), 475 (7.6), 384 (87.2), 368 (12.7), 206 (2.0), 180 (4.0), 165 (7.4), 91 (2.4); HRMS calcd for $C_{34}H_{25}N_3O_2S$: 539.17, found: 539.17; Element analysis calcd (%) for $C_{34}H_{25}N_3O_2S$: C 75.67, H 4.67, N 7.79, O 5.93, and S 5.94; found: C 75.29, H 4.67, N 7.80, O 6.02, and S 5.78.

2.3. Computational details

All molecular structures were fully optimized using the hybrid B3LYP functional method [32], in combination with 6-31G(d,p) Gaussian basis set. For each optimized structure a frequency analysis at the same level of theory was used to verify that it corresponds to a stationary point in the potential energy surface. As the use of diffuse functions is essential for accurate determination of the energetics, particularly for ion radicals and excited states [33], to perform a single-point calculation on the basis of B3LYP/6-31G(d,p) optimized structures. The excited-state properties were calculated with the time-dependent density functional theory (TD-DFT) [34–36] formalism, using the optimized ground state geometries. TD-DFT in combination with the B3LYP hybrid functional and the 6-31G (d,p) basis set has previously been shown to provide accurate energies for excited states within 0.2 eV (5 kcal mol^{-1}) [37]. All calculations were performed with the Gaussian 03 package of programs.

In addition to DFT calculations, semi-empirical methods offer an attractive alternative for studying potential energy surfaces in ground and excited states. Procedures such as the AM1 method [38,39] allow examination of potential energy surfaces without geometric assumptions. With inclusion of limited configuration interaction, especially through the single and pair double excitation (PECI) procedure [40], spectral properties of several conjugated organic systems have been shown to be reliably reproduced [41,42]. Therefore, the spectral properties of ESIPT dyes have been simulated using AM1/PECI = 8 calculations in order to guide the synthetic efforts towards materials with enhanced performances and to help with the interpretation of the experimental data.

3. Results and discussion

3.1. Synthesis and characterization of phenanthroimidazoles

Scheme 1 outlines the three synthetic routes that were utilized for synthesis of the phenanthroimidazoles. Key step in all the routes is the formation of the phenanthroimidazole ring from the corresponding substituted aryl precursors using a slightly modified procedure of the Steck and Day method [43]. The condensation reaction of phenanthroquinone with salicyladehyde was conducted in the presence of excess ammonium acetate as the source of the imidazole nitrogen atoms in glacial acetic acid for a reaction time of 4 h at 110 °C to afford HPhI in 53% isolated yield. Unlike for 1,2-diphenyl-1,2-ethanedione, which forms only the imidazole condensation product, phenanthroquinone or phenanthroline-5,6-dione yields both imidazole and oxazole products competitively [44,45]. The rigidity and co-planarity of the carbonyl groups in the fused-ring starting materials enabled close proximity of heteroatoms towards competitive cyclization of NN̂ diimine and NÔ keto-imine intermediates. In order to alter the electronic environments of the five-membered imidazole and six-membered phenol rings of the 2-(1H-imidazol-2-yl)phenol nucleus, a rational reaction of appropriate aryl aldehydes (salicyladehyde, 2-nitrobenzaldehyde) with phenanthroquinone was considered for the preparation of 1,2-diphenyl-phenanthro[9,10-d]imidazoles. Both HPPhI and NPPhI were readily synthesized according to the reported literature procedure of 2-(1,4,5-triphenyl-imidazol-2-yl)-phenol [20] in good yields 60% and 95%, respectively. The methoxy analogues MPhI and MPPhI in which the absence of free phenolic hydroxyl group blocks the formation an intramolecular hydrogen bond were obtained from corresponding hydroxyl phenanthroimidazoles HPhI and HPPhI with equimolar amount of CH_3I and K_2CO_3 in DMF in high yields 94% and 81%, respectively. Through the palladium-catalyzed hydrogenation of the nitro group of NPPhI

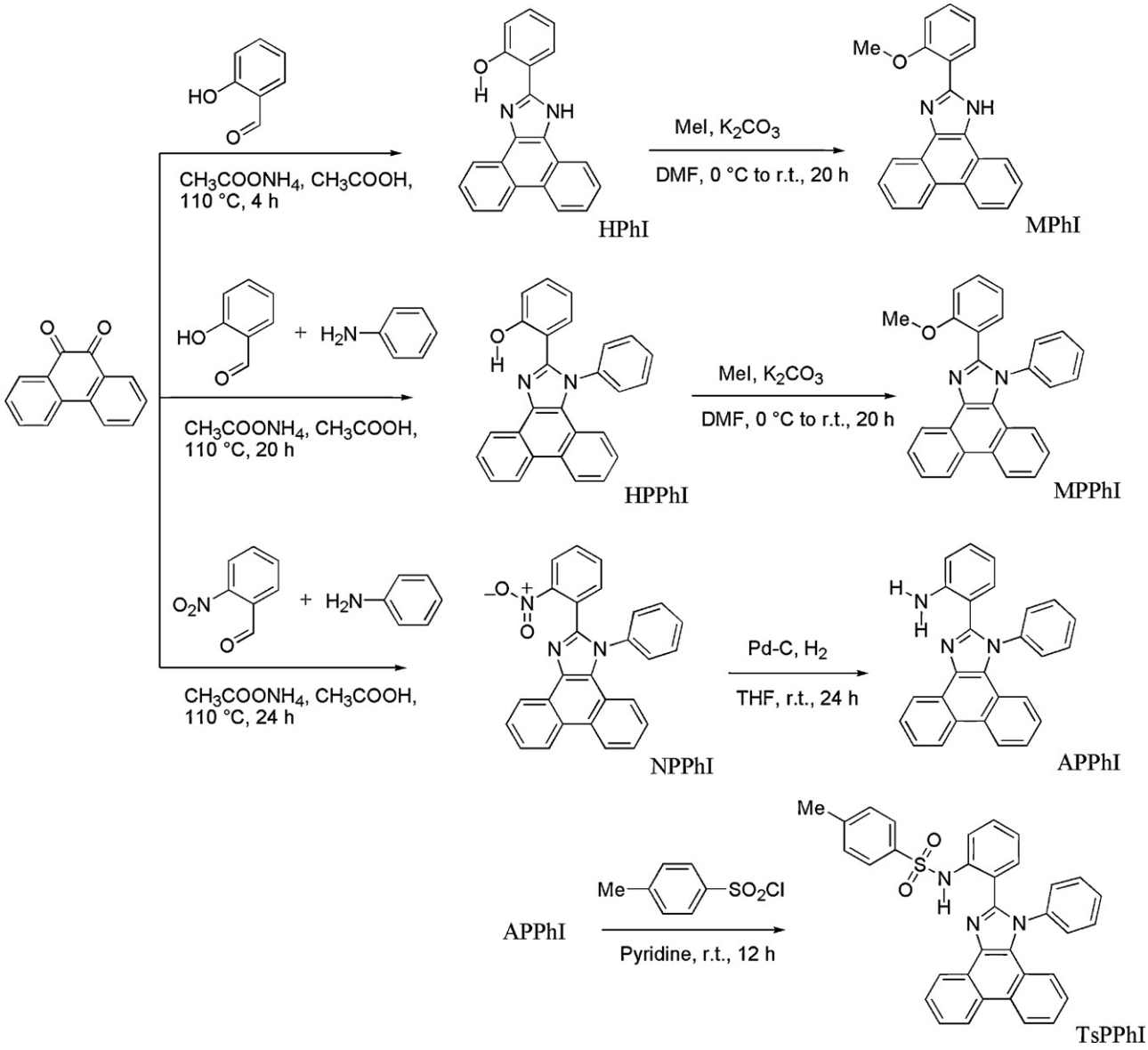

Scheme 1. Synthetic routes for preparation of the phenanthroimidazole derivatives.

at ambient pressure gave APPhI in 96% yield. Subsequently, the condensation reaction of APPhI with *p*-toluenesulfonyl chloride in anhydrous pyridine at room temperature provided TsPPhI in 85% yield. The easy synthetic procedures and relatively high yields of the presented 1,2-diphenyl-phenanthroimidazole derivatives are, therefore, promising for large-scale production. All synthesized phenanthroimidazole derivatives were carefully characterized by ^{1}H NMR, ^{13}C NMR, MS-EI/HRMS, and elemental analysis.

The molecular structures of phenanthroimidazoles, *o*-substituted with electron-donating (—OH, —OMe, —NH_2, and —$NHSO_2R$) or electron attracting (—NO_2) groups in the 2-phenyl ring were designed on the frame of an imidazole ring with phenyl groups attached to it. The optimized geometry of these phenanthroimidazoles in the ground state was investigated with quantum chemical calculations. Ground state geometry optimizations were obtained by density functional theory (DFT) calculation using Becke's three-parameter function combined with Lee, Yang, and Parr's correlation function (B3LYP) [32]. From the calculated molecular conformations of mono- and di-aryl phenanthroimidazoles shown in Fig. S1, it is noted that the diaryl phenanthroimidazoles are non-planar and very twist molecular structure, whereas mono-aryl substituted phenanthroimidazoles are coplanar. The torsion angles between the imidazolyl group and the neighboring 2-phenylene group in HPhI, HPPhI, MPPhI, and TsPPhI molecules were estimated as (φ_2) 0, 9.4, 96.8, and 43.6 whereas the torsion angles between the imidazolyl group and the neighboring 1-phenylene group in HPPhI, MPPhI, and TsPPhI molecules were estimated as (φ_1) 85.0, 71.9, and 99.0, respectively. The calculated bond lengths, angles, and hydrogen-bond parameters are provided in Table 1.

The most striking feature of the TsPPhI structure is the parallel orientation of the tosyl and phenanthroimidazole rings, leading to significant intramolecular π-stacking interactions. The two planes deviate only by 12.7° from a parallel orientation with a distance of approximately 4.69 Å. The unusual geometry is best revealed with a projection along the interannular bond axis, which shows a dihedral angle of 43.6° between the phenanthroimidazole ring and the attached phenyl ring. The substantial out-of-plane twist of the aryl–phenanthroimidazole unit is presumably a result of the π-stacking interaction, which is most effective with a planar orientation of the aryl rings. This assumption is further supported by the geometry reported for 2-(2′-tosylaminophenyl)benzimidazole, in

Table 1
Energetic characterization of enol–keto and amine–imine (N_{syn}–T_{syn}) tautomers in ground (S_0) and excited (S_1) states in parenthesis.

Conformer	HPhI enol (N_{syn})	HPhI keto (T_{syn})	HPPhI enol (N_{syn})	HPPhI keto (T_{syn})	TsPPhI amine (N_{syn})	TsPPhI imine (T_{syn})
Energy/hartree	−993.4820	−993.4639	−1224.5265	−1224.5098	−2023.6001	−2023.5802
Rel. energy/kcal mol^{-1} S_0 (S_1)	0(2.7)	11.37 (0)	0(3.53)	10.47 (0)	0(6.31)	12.51 (0)
Bond length/Å O—H	0.995	1.584	0.998	1.512	–	–
N—H	–	1.046	–	1.045	1.027	1.618
=N···H	1.724	–	1.661	–	2.036	–
N—O	2.621	2.483	2.564	2.437	–	–
N—N	–	–	–	–	2.878	2.499
C—C (interannular bond length/Å)	1.455	1.419	1.467	1.433	1.474	1.444
φ_1 (1′-ph)/deg	–	–	85.0	89.6	99.0	92.8
φ_2 (2′-ph)/deg	0	0	9.4	0	43.6	3.2
φ_3 (IHB)/deg	0	0	3.0	0.2	14.0	5.9
μ/D	3.62	6.32	4.93	6.80	2.09	11.77
Excitation energy/nm	342.1	411.4	343.6	413.0	330.3	422.2
Oscillator strength (f)	0.357	0.148	0.312	0.147	0.242	0.240

which the two aryl rings are essentially coplanar with a small dihedral angle of ∼3.3° [14]. Additional geometric constraints induced by the π-stacking interaction can be observed along the sulfonamide backbone. Whereas the bond angle tosyl C—S—N of 109.8° is in the typical range for aromatic sulfonamides, the S—N—C angle of 114.7° is considerably more acute than 124–125°, which is typically found for similar compounds [46].

Owing to their rigid and non-coplanar structures diaryl phenanthroimidazoles are expected to decrease the intermolecular stacking efficiency due the steric crowding. Therefore, it is expected to exhibit good solubility without loss of their excellent thermal properties. The diaryl substituted phenanthroimidazoles exhibited high melting points (T_m) around 184–266 °C. In addition, distinct glass transition temperature (T_g) could be observed for HPPhI, MPPhI, and TsPPhI at 68.0, 78.3, and 99.0 °C, respectively whereas the T_g of HPhI and MPhI was not detectable (Tables 2 and S1). Among them, HPPhI shows a relatively lower T_g and T_m at 68.0 and 184 °C, respectively. This is probably because of the lower rotational barrier of the central phenylene group in HPPhI compared with other diaryl substituted phenanthroimidazoles like TsPPhI. All of the diaryl phenanthroimidazoles showed no crystallization or phase transition behavior upon heating beyond T_g. This suggests that the diaryl phenanthroimidazoles have amorphous nature in condensed state, which may greatly benefit the formation homogeneous and amorphous films through thermal evaporation.

All the dyes exhibit the wavelength absorption peaks around 260 ± 5, 330 ± 10, 360 ± 5 nm in their solutions (2×10^{-6} to 5×10^{-6} M) of chloroform, acetonitrile, 1-propanol, and methanol at room temperature, which can be considered to be absorptions belonging to π–π* transitions on the basis of extinction coefficients ($\varepsilon_{\lambda_{max}}$, Tables 2 and S1) and oscillator strengths (f) from molecular orbital (MOs) calculation (Table 1). The molar absorption coefficients range between 12,580 and 38,100 cm^{-1} M^{-1}, which is in the typical range for allowed π–π* transitions. Regardless of the solvent polarity, all spectra show a distinct vibrational structure, which is typical for 9,10-phenanthroimidazole [47] and 2-phenyl-9,10-phenanthroimidazole (PhI) [48] rigid molecular framework. Considering the 9,10-phenanthroimidazole or PhI nucleus as the fundamental skeleton of the chromophores, absorption data shows that conjugation of the π system is extended by the electronic substituents on the 1,2 positions of the imidazole ring, leading to bathochromic and hyperchromic shifts. The close similarity of all spectra in different solvents indicates that the ground state structure of these phenanthroimidazoles must be very similar in all solvents. Even in protic and very polar solvents such as 1-poropanol or methanol, no significant change that might imply the presence of an additional ground state conformation or rotamer was observed. In general, absorption peaks were slightly blue shifted in methanol compared to those in chloroform. When the absorption positions of dyes in $CHCl_3$ and 1-propanol were compared, the peaks hardly showed a response to solvent polarities (*i.e.* 0–3 nm shifts). Polarities of the solvents might not be important in affecting electronic properties of the compounds, and this observation is in agreement with the prominence of a π–π* nature of transition to the excited states rather than n–π*. In the solid thin films, the chromophores maintained similar absorption spectral positions to those of the solution.

Tables 2 and S1 list absorption maxima and optical bandgaps of all synthesized phenanthroimidazoles. This data indicates that the optical bandgap (E_g) of aryl and diaryl phenanthroimidazole derivatives is lower than that of parent PhI (E_g = 3.522 eV in CH_3CN) [47,48]. As shown in Tables 2 and S1: HOMO energy levels of these dyes were found to be around 5.06–5.61 eV. This difference can be attributed to the electron donating ability from different charge transporting substituents on the phenanthroimidazole moiety. For example with strong electron donating arylamine, APPhI possesses the highest HOMO energy level among these dyes. Similarly, MPPhI has second small oxidation potential and the second high HOMO energy level next to that of APPhI. This is because the anisole moiety is less electron rich than that of aniline. On the other hand, it is reasonable to find NPPhI with highest oxidation potential and the lowest HOMO energy level among phenanthroimidazoles dye due to its built-in electron withdrawing —$ArNO_2$ moiety. The ionization potential (*IP*) of electron donating substituted derivatives is smaller than those of electron withdrawing groups. It suggests that the electron donating groups favors the decrease in the ionization potential (*IP*).

Fluorescence data and comparative overlays of emission spectra of all synthesized compounds are presented in Tables 2, S1, and Figs. 2B, D and S2–S3, respectively. The excitation spectra are insensitive toward alteration of the emission wavelength at which the spectra were acquired (data are not shown). The peak excitation wavelengths are also identical with the measured maxima of the UV spectra. This again is consistent with a single ground-state rotamer, which is responsible for the abnormally large Stokes' shifted emission band. It could be noticed that non-ESIPT chromophores (MPhI, MPPhI, APPhI, and NPPhI) gave normal Stokes' shifted emissions in the deep blue region of the visible spectrum (366–418 nm) while intramolecularly hydrogen-bonded chromophores HPhI, HPPhI and TsPPhI produced mainly large Stokes' shifted tautomer emissions in the blue-green region (464–490 nm) as a result of ESIPT process. The emission spectra of the phenanthroimidazoles vary with the increase of the polarity and hydrogen-bonding capability of the solvents; the band maxima of the tautomer emissions get blue shifts, whereas the band maxima of the normal emissions get red shifts. In comparison with the solution PL spectra, the emission of respective phenanthroimidazoles in the solid state is slightly blue-shifted with a reduced FWHM

Table 2
Thermal, photophysical and electrochemical properties of phenanthroimidazole ESIPT chromophores.

Sample	In solution and thin film (PMMA in 5 wt% of dye)	λ^{ab}, nm ($\log \varepsilon_{max}$)	λ^{fl}, nm (Φ^{fl}) $\times 10^{-2}$	T_g[a] (°C)	IP[b] (eV)	E_{oxd}[c] (eV)	HOMO[c] (eV)	LOMO[d] (eV)
HPhI	$CHCl_3$	260 (4.844), 342.8 (4.539), 363 (4.581)	367, 384, 407(sh) (0.07), 478 (4.96)	–	8.269	−1.600	−5.610	−2.194
	CH_3CN	256.7 (4.818), 334 (4.481), 340 (sh), 361 (4.497)	365, 384.7, 404 (sh) (0.13), 482 (0.75)					
	1-Propanol	257.7 (4.820), 341 (4.496), 361 (4.557)	365, 384.7, 404 (sh) (0.31), 479.6 (1.75)					
	Thin film	344, 364	391, 480 (29.10)					
HPPhI	$CHCl_3$	264 (4.749), 334.5 (4.385), 347 (sh), 364.5(4.335)	372, 388, 468 (14.69)	68.0	8.226	−1.289	−5.298	−1.896
	CH_3CN	261.6 (4.775), 331 (4.391), 343.7 (sh), 362 (4.286)	366, 373, 390 (0.01), 469 (1.23)					
	1-Propanol	261 (4.803), 332 (4.315), 344 (sh), 362.4 (4.251)	366, 378, 465 (5.39)					
	Thin film	333.5, 346.2, 364.4	375, 392, 464 (38.5)					
TsPPhI	$CHCl_3$	258.7 (4.834), 322 (4.263), 338, 356 (4.093)	366, 384 (1.68), 487 (48.76)	99.0	8.283	−1.440	−5.450	−1.967
	CH_3CN	255.6 (4.844), 282 (sh), 303 (sh), 319 (4.252), 337, 354 (4.049)	364, 383 (1.52), 490 (20.65)					
	1-Propanol	256 (4.844), 283 (sh), 320 (4.212), 337, 353.9 (4.028)	364, 382 (4.57) 488 (33.33)					
	Thin film	280, 305, 321.6, 338, 356	368, 383, 403 (sh) 470 (67.85)					

[a] Glass transition temperature (T_g) was obtained from differential scanning calorimetry (DSC) measurements.
[b] Ionization potential (IP) was calculated by AM1 method.
[c] All electrochemical oxidation potentials were measured by cyclovoltammetric method (CV) in dichloromethane solution using ferrocene/ferrocinium as the internal reference electrode at a scan rate of 100 mV s^{-1} and calculating the HOMO levels.
[d] The LUMO (lowest unoccupied molecular orbital) levels were estimated by subtracting absorption energy (optical bandgap) from HOMO levels.

(full-width at half-maximum) of ~3–4 nm; this reduced FWHM implies that there would be weak aggregation involved in their solid state [49].

It is interesting to note that the emission maximum of TsPPhI appears at a longer wavelength with a shift of 20 nm compared to HPPhI. This indeed would be consistent with an excited-state interaction of the phenanthroimidazole chromophore with the arenesulfonamide group, which results in a more stabilized excited state and therefore a lower emission energy (Supporting information Fig. S1). Because the pK_a value of aryl-substituted sulfonamides are comparable to their phenol analogues, the ESIPT process in TsPPhI is expected to be similarly efficient as for HPPhI. In all solvents, an intense large Stokes' shifted emission band was observed, which can presumably be attributed to the sulfonimino tautomer T_{syn}* (Fig. 1). Initial measurements of ESIPT dyes showed a weak emission band at higher energy in most solvents, which we interpreted with the presence of the *trans*-rotamer N_{anti} (Fig. 2B, D). Nevertheless, as quantum chemical calculations suggested, the ground-state equilibrium should be exclusively dominated by the *cis*-rotamer N_{syn}, and therefore the normal emission band was a surprising observation.

The solid state fluorescence quantum efficiency of HPhI, HPPhI, and TsPPhI reaches to the very high value of 29.10%, 38.50%, and 67.85%, respectively, increasing up to 2–6 folds compared to their solutions (Fig. 3 and Tables 2, S1). Also an interesting fact is that, unlike for any other compound in the studied series, compound TsPPhI displayed a very brilliant solid film photoluminescence in the blue-green region of the visible spectrum at room temperature. Besides electronic effects, there is probably an interesting steric effect of the multiple phenyl substituents on molecular arrangements in solid state, and is most probably interacts in an "offset face-to-face" fashion with another imidazolyl ring of a contiguous moiety in TsPPhI compared to HPPhI. Possibly, the relative small intermolecular π–π overlapping areas of these diaryl phenanthroimidazoles compared with that of mono-aryl phenanthroimidazoles is probably a key factor that accounts for their high fluorescence quantum yields in the solid state and in the thin film. The corresponding intramolecular motions and relative free-rotation of end phenyl groups in solution may be the origin of weak fluorescence (*vide infra*). In the solid state, the free-rotation occurring in both compounds in solution will be depressed due to the intermolecular interaction, which is beneficial to enhanced fluorescent efficiency.

3.2. Quantum chemical calculations and photophysical properties

To study further about the relationship between their molecular structures and optical properties, the geometrical parameters of N_{syn}–T_{syn} tautomers and their energy-minimized, preferred conformations were calculated by DFT using B3LYP/6-31G(d,p) [32] and semi-empirical using AM1 calculations [38,39]. The geometry optimization in the S_0 and S_1 of N_{syn}, T_{syn} and transition state (TS) of the phenanthroimidazoles was performed and respective parameters are listed in Table 1. As shown in Table 1, in the S_0 and S_1 for N_{syn} form, the distance of N···H in HPhI, HPPhhI, and TsPPhI was about 1.66–2.03 Å. It is well known that H-bond is short distance force in essence; hence the H-bond force between H and N should be operating in the N_{syn} form of these dyes. On the other hand, the distance of N···H was too short in the S_0 and S_1 for the T_{syn} form, even up to about 1.51–1.62 Å. Generally, the $N_{syn} \rightarrow T_{syn}$ tautomerization brought a variation of the chemical bond length of phenol or sulfonamide ring. For instance, the maximum of the difference between the bond lengths of phenolic O—H in the N_{syn} form of HPhI, HPPhI was <0.01 Å, while the value in the T_{syn} form increased to 0.14 Å, implying that aromaticity of this ring in the T_{syn} form was lost because of the internal proton transfer.

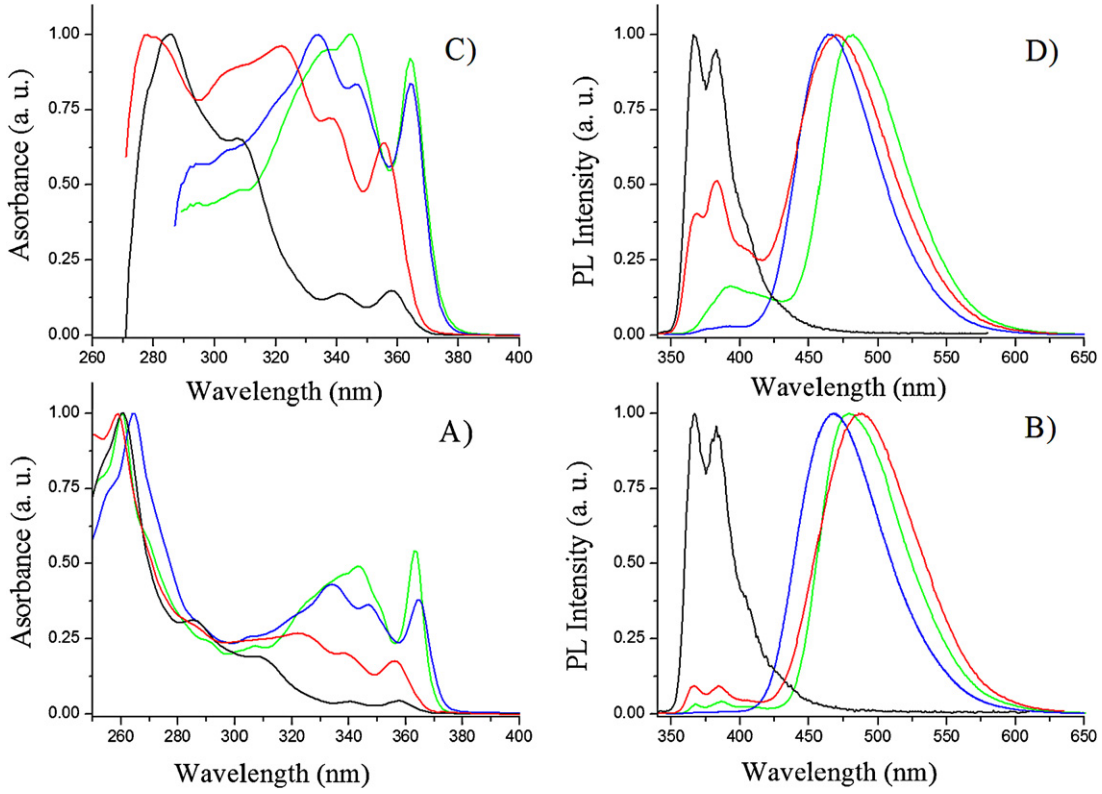

Fig. 2. (A) Normalized UV–vis absorption and (B) photoluminescence spectra of HPhI, green; HPPhI, blue; MPPhI, black; TsPPhI, red in $CHCl_3$; (C) normalized UV–vis absorption and (D) photoluminescence spectra of HPhI, green; HPPhI, blue; MPPhI, black; TsPPhI, red in a polymethylmethacrylate (PPMA) solid film doped with 5 wt% of each dye. (For interpretation of the references to colour in this figure legend, the reader is referred to the web version of the article.)

Interestingly, during the ESIPT process ($N_{syn}^* \rightarrow T_{syn}^*$) the observed change in the bond lengths of sulfonamide N—H in TsPPhI was large (*ca.* 0.42 Å) as compared to HPhI and HPPhI (*ca.* 0.14 Å) which in turn more polar in nature (μ = 11.77 D) and manifest with decrease in rate of ESIPT reactions. Again the stable ground state geometry of N_{syn} of HPPhI and TsPPhI had twisted bond φ_2 (2′-ph) by *ca.* 9.4° and 43.6° at B3LYP/6-31G(d,p) level respectively. Dihedral angle was decreased to *ca.*0° and 3.2° respectively during $N_{syn} \rightarrow T_{syn}$ tautomerization, reflecting that the extent of molecular distortion was reduced. While in the excited state of HPhI, the tautomers remained essentially in the same plane. In a system with a great delocalization of π-electron, the torsion angle decided whether the molecule could be well-conjugated. Consequently, the small twisted configuration in the excited state allowed the extension of the conjugated π-electron in the entire molecular framework, and the energy barrier in the ESIPT process caused by the ground state twisting was reduced. It was favorable to undergo ESIPT for HPPhI and TsPPhI.

The plots of the potential curves of internal proton transfer in S_0 and S_1 states of HPPhI as a function of O—H distance were performed using AM1/PECI = 8 and presented in Fig. 4,

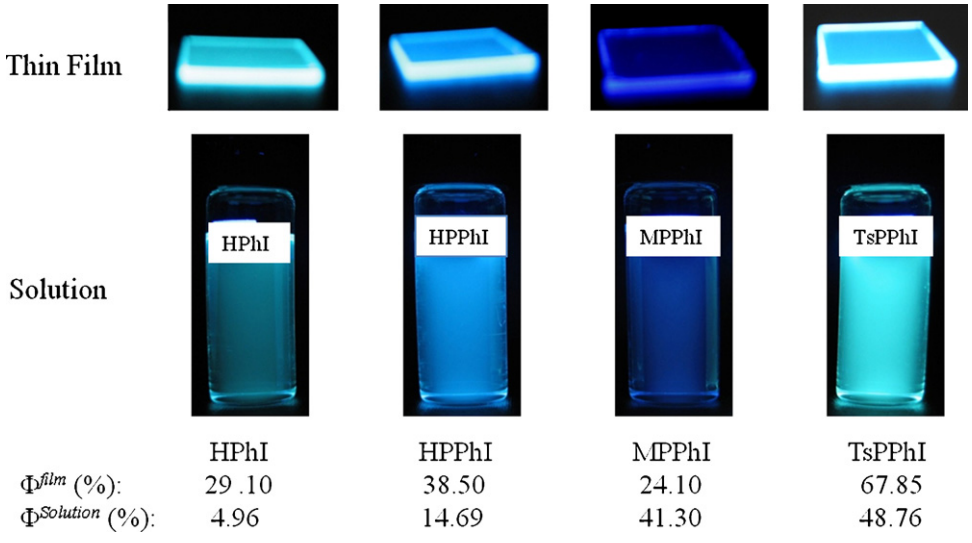

Fig. 3. PL images of PMMA film doped with 5 wt% dye on the wedged quartz plate and solution and their absolute photoluminescence quantum yield (Φ^{PL}).

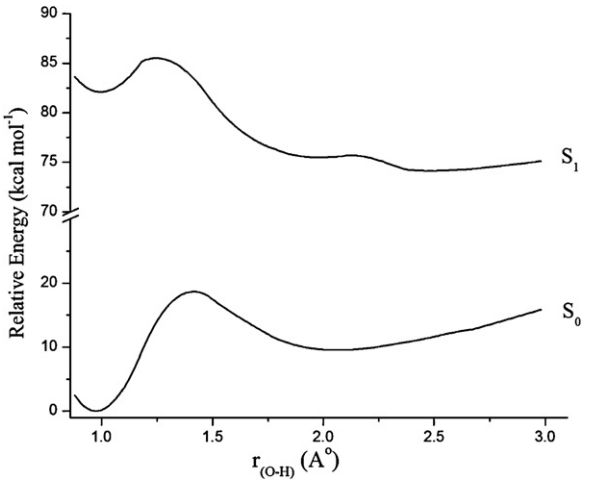

Fig. 4. The internal proton-transfer reaction potential energy curves of HPPhI relaxed along the O—H distance for the ground and excited state using AM1/PECI = 8 calculation.

which shows clearly that the N_{syn} form is most stable in the S_0 state whereas the T_{syn} form is most stable in the S_1 state. ΔE (energy difference between N_{syn} and T_{syn}) again reveals that T_{syn} form has a higher energy than N_{syn} form in S_0 state as the aromatic ring is broken by proton transfer. The activation barrier for $N_{syn} \rightarrow T_{syn}$ in S_0 electronic state is 18.55 kcal mol^{-1}, large enough to make the ground state intramolecular proton transfer (GSIPT) unviable under thermal conditions, whereas upon photoexcitation, much smaller interconversion barrier ($N_{syn}^* \rightarrow T_{syn}^*$) of 3.32 kcal mol^{-1} in S_1 state preferably allows ESIPT to give the large Stokes' shifted fluorescence emission (*ca.* 104.9 nm and 6605 cm^{-1}). After decaying to the ground state, the phototautomer T_{syn}^* reverts to the original N_{syn} *via* reverse proton transfer barrier ($\Delta E_r^{\#}$) of 8.97 kcal mol^{-1}. This implied that although the occurrence of GSIPT from $N_{syn} \rightarrow T_{syn}$ should be very difficult, the reverse proton transfer process from $T_{syn} \rightarrow N_{syn}$ could take place easily, which was much favorable for ESIPT occurrence. Finally, the protons transfer from T_{syn} to the starting N_{syn} in thermal processes in S_0 states to finish the cyclic four-level photophysical scheme ($^1N_{syn} \rightarrow {}^1N_{syn}^* \rightarrow {}^1T_{syn}^* \rightarrow {}^1T_{syn} \rightarrow {}^1N_{syn}$), immediately after photoexcitation of the intramolecular H-bonded molecules. Therefore, an abnormally large Stokes shift without self-absorption is detected, providing an ideal scheme for UV-photostabilizers or proton transfer lasers.

The electron distribution of the frontier orbitals reflects the electron transition characteristics. Seen from Fig. 5, the HOMO and LUMO of substituted phenanthroimidazoles exhibited π-type symmetry. From HOMO to LUMO, the electron density distribution displayed the transfer from phenolic ring to phenanthroimidazole moiety. The calculated long wavelength absorption peak of HPhI (*ca.* 342.1 nm, oscillator strength (*f*) = 0.357), HPPhI (*ca.* 343.6 nm, oscillator strength (*f*) = 0.312), TsPPhI (*ca.* 330.3 nm, oscillator strength (*f*) = 0.242) is a mixture of different transitions, *e.g.*, HOMO → LUMO, HOMO → LUMO + 1, HOMO → LUMO + 2, *etc.* The shapes of the HOMOs look very similar to each other for these molecules. However, the LUMO + 1 of HPhI, HPPhI and LUMO + 2 of TsPPhI are delocalized through the acceptors and π-bridges. This change in the electron density acts as a driving force for the very fast intramolecular proton transfer in these compounds upon excitation to the S_1 state. Thus, the phenolic ring had smaller electron density in the excited state, which was driving force for the occurrence of proton transfer for HPPhI in the excited state. Hence, the HOMO → LUMO transition could be ascribed to π–π* excitation with internal charge transfer character [50].

The Mulliken net atomic charge population of the key atoms (O—H, N—H, and N—O) of HPPhI and TsPPhI are shown in Fig. 6.

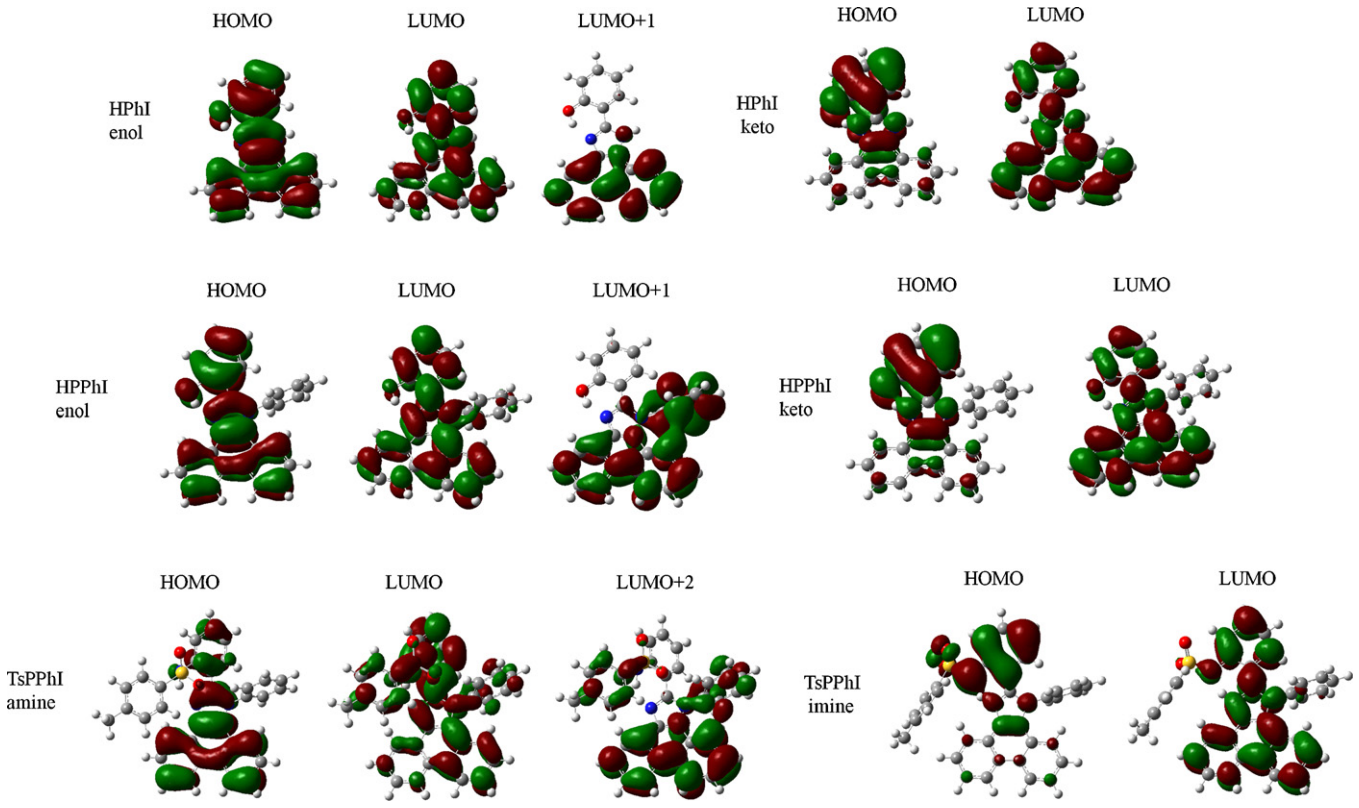

Fig. 5. Calculated contour plots of frontier orbitals of enol (N_{syn}) and keto (T_{syn}) form of ESIPT chromophores (TD-DFT method at the B3LYP/6-31G(d,p) level).

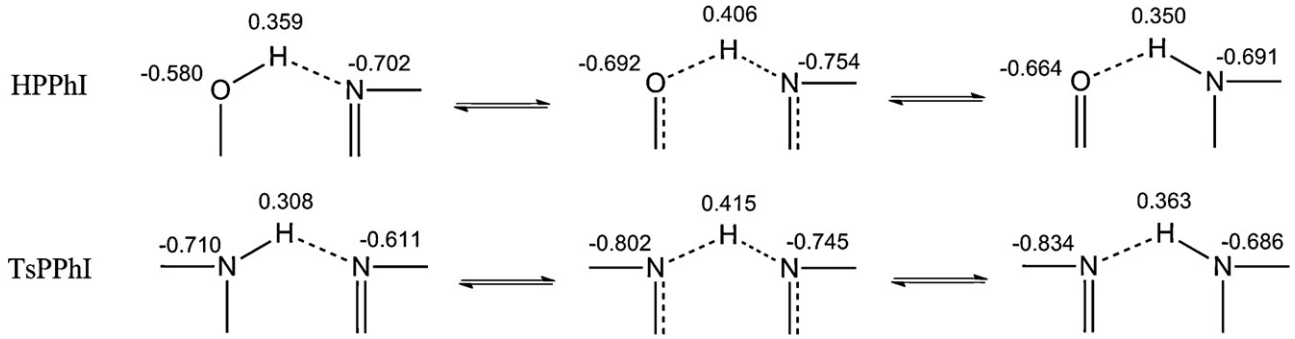

Fig. 6. The calculated Mulliken net atomic charge population of the key atoms of HPPhI (at the top) and TsPPhI (at the bottom) involving tautomerization (N_{syn}–TS–T_{syn}) using B3LYP/6-31G(d,p) method.

Remarkably, as per expectation, hydrogen atom had high positive charge, which indicated that it was a "real proton" transfer if ESIPT or GSIPT took place. Interestingly, the positive charge of hydrogen experienced increasing and then decreasing during intramolecular proton transfer both in ground and excited states, reaching the maximum at TS because of largest hydrogen-bond strength. While N_{syn} was excited to N_{syn}^*, the part of negative charge was transferred from the hydroxyl to the imino group, which resulted in the change of the "force balance" of hydrogen bond. Consequently the negative charge of the proton donor decreased (more acidic), and the negative charge of the proton acceptor increased (more basic), which enhanced the change of geometry in the excited state and prompted the ESIPT occurrence for photoreactive hydrogen-bonded chromophore. Table S2 shows that the dipole moments centralized on the *Y*-dimension and the electronic transition led to the changes in the charge distribution, which was accompanied by the increase of the molecular dipole moments in the excited state. As compared with HPPhI, owing to the great changes of the dipole moment of on the *X*- and *Y*-dimension in both the ground and the excited state, the dipole moment of TsPPhI of normal form was lowered, but the dipole moment of tautomer form was enhanced greatly, thus the dipole moment difference of tautomers of TsPPhI exhibited much large changes in both the ground and excited state than HPPhI (Table S2 and Fig. S5). This meant that large change of charge geometry occurred due to internal proton transfer, which in turn indicated a bit difficult to undergo GSIPT or ESIPT as manifested by relatively larger intensity ratio of normal to tautomer emission in TsPPhI than that in HPPhI.

Recent quantum chemical modeling studies on salicylanilides [51], salicylideneaniline (SA) [52] show that ESIPT occurs from a planar N_{syn}^* which gives a planar T_{syn}^* (*cis*-keto*). This planar T_{syn}^* is not stable and undergoes out-of-plane torsion which is the precursor of *syn-anti* (*cis–trans*) isomerization to the T_{anti} (*trans*-keto) photoproduct. Thus one hypothesis for the two fluorescent T_{syn}^* (*cis*-keto*) is a planar and a nonplanar isomer or different nonplanar isomers. The bulky phenyl or tosyl group can stabilize them and favor the existence of two fluorescent T_{syn}^* species in comparison with HPhI. The difference in fluorescence intensity among HPhI, HPPhI, and TsPPhI in solid state can be well explained by their different classes: as mentioned above, the T_{syn}^* in TsPPhI does not lead to the T_{anti} (*trans*-imine) photoproduct which relaxes by nonradiative decays (internal conversion) but fluoresce to T_{syn} ground state. In contrast, relatively fast formation of the T_{anti} photoproduct in mono-aryl phenanthroimidazole HPhI reduces the fluorescence of the T_{syn}^*. In solution, however, both mono- and di-aryl phenanthroimidazoles are relatively stabilized an intramolecular charge transfer (ICT) process in T_{syn}^* might induce the interannular bond rotation, leading to a non-emissive, twisted excited state T_{ICT}^* after the ESIPT, which explains the weak fluorescence of the T_{syn}^*. Thus, it can be stated that the substituents in the ESIPT molecules that favor the ICT from the proton donor to the proton acceptor moiety will increase the nonradiative decay and, consequently, decrease the fluorescence quantum yield.

Restricted intramolecular/intermolecular motion [20–28] has been suggested as one of the most significant mechanisms of aggregation-induced emission enhancement (AIEE) phenomenon. In dilute solutions of molecular dispersed phenanthroimidazole dyes, two end-substituted phenyl units of the molecule could rotate freely around the single bonds and the radiative decay would be effectively restricted by this kind of intramolecular torsion. While in the aggregate state, the intramolecular rotation and torsion were greatly impeded and therefore the non-radiative decay channel was effectively restricted, which in turn populated the irradiative state of the excited molecules and resulted in a great increase of fluorescence. Hence, it was easy to understand why the molecularly dispersed dilute solutions of phenanthroimidazoles were so weakly luminescent while their solid particles and aggregates were highly emissive. All these results in agreement with the proposed mechanism for the intramolecular H-bonded compounds HPhI, HPPhI, and TsPPhI in dilute solution undergo an excited state charge transfer coupled proton transfer depicted in Fig. 1. Upon excitation of N_{syn} an ESIPT process takes place to give T_{syn}^* fluorescent species, after which the excited tautomer undergoes a large-amplitude conformational change associated with a charge migration from deprotonated phenol or sulfonamide moiety to the protonated imidazole moiety, yielding the non-fluorescent charge-transfer intermediate T_{ICT}^*, which probably deactivates very fast [10]. The electronic and geometric structure of T_{ICT}^* in Fig. 1 is hypothetical, not only about the nature of the conformational change experienced by T_{syn}^* but also in relation to the charge distribution. Accordingly, the fluorescence enhancement in the solid state is due to the prevented T_{ICT} by kinetic constraint which blocks large amplitude twisting motion about the interannular C—C bond (torsion angle, φ_2) along the ESIPT reaction coordinate.

4. Conclusion

Seven phenanthroimidazoles derivatives (HPhI, MPhI, HPPhI, MPPhI, NPPhI, APPhI and TsPPhI) have been synthesized and detailed studies of their electronic structures, photophysical and electrochemical properties are presented. The branched 1,2-diphenyl-phenanthro[9,10-*d*]imidazoles are more emissive than their linear 2-phenyl-1*H*-phenanthro[9,10-*d*]imidazole analogs, both in solution and when aggregated, presumably because of increased π-electron contributions to the electronic structure of the molecule, as well as restricted nonradiative deactivation resulting from less facile rotational deactivation *via* the interannular C—C bond (torsion angle, φ_2). The quantum chemical studies reveal that the formation of non-fluorescent isomers (T_{ICT}^*) of 1,2-diphenyl phenanthroimidazoles was effectively suppressed

in the solid state due to the bulky substituents preventing a large-amplitude conformational change in the excited-state. The ESIPT dyes containing branched 1,2-diphenyl-phenanthro[9,10-*d*]imidazole groups showed excellent thermal properties with high T_g (around 68–99 °C) and an efficient large Stokes' shifted emission at *ca.* 464–490 nm with very high fluorescence quantum yield ~39–68% in the neat solid films without suffering from concentration self-quenching. The molecular design concept established in this study should provide guidelines for fine-tuning the emission properties of this class of ESIPT fluorophores, which is beneficial for developing a new class of advanced optoelectronic applications.

Supplementary information

Electronic supplementary information (ESI) available: ^{1}H and ^{13}C NMR spectra of pure phenanthroimidazoles, DSC traces, cyclic voltammetry, UV–vis absorption and photoluminescence, optimized geometries of keto–enol (HPhI and HPPhI) and amine–imine (TsPPhI) tautomers, atom coordinates and absolute energies of the computed structures, HOMO–LUMO orbital's of ESIPT, and non-ESIPT phenanthroimidazoles MPhI, MPPhI, NPPhI, APPhI upon photo excitation.

Acknowledgements

The author is gratefully acknowledged to Professor Soo Young Park, Department of Materials Science and Engineering, Seoul National University, South Korea, for useful comments and assistance in the determination of the photoluminescence quantum yields of phenanthroimidazole dyes in solid state. I also thank Professor Hassan S. Bazzi, Department of Chemistry, Texas A&M University at Qatar, for giving me technical knowledge in several fields.

Appendix A. Supplementary data

Supplementary data associated with this article can be found, in the online version, at http://dx.doi.org/10.1016/j.jphotochem.2012.05.018.

References

[1] J.P. Richard, T.L. Amyes, Current Opinion in Chemical Biology 5 (2001) 626–633;
M. Burnworth, S.J. Rowan, C. Weder, Chemistry: A European Journal 13 (2007) 7828–7836;
E.W. Debler, S. Ito, F.P. Seebeck, A. Heine, D. Hilvert, I.A. Wilson, Proceedings of the National Academy of Sciences of the United States of America 102 (2005) 4974–4989.
[2] D. Altschuh, S. Oncul, A.P. Demchenko, Journal of Molecular Recognition 19 (2006) 459–477;
S.Y. Reece, J.M. Hodgkiss, J. Stubbe, D.G. Nocera, Philosophical Transactions of the Royal Society B: Biological Sciences 361 (2006) 1351–1364;
D. Stoner-Ma, A.A. Jaye, K.L. Ronayne, J. Nappa, S.R. Meech, P.J. Tonge, Journal of the American Chemical Society 130 (2008) 1227–1235.
[3] M.J. Paterson, M.A. Robb, L. Blancafort, A.D. DeBellis, Journal of Physical Chemistry A 109 (2005) 7527–7537.
[4] S.-J. Lim, J. Seo, S.Y. Park, Journal of the American Chemical Society 128 (2006) 14542–14547.
[5] A.S. Klymchenko, V.V. Shvadchak, D.A. Yuschenko, N. Jain, Y. Mély, Journal of Physical Chemistry B 112 (2008) 12050–12055;
T. Ozturk, A.S. Klymchenko, A. Capan, S. Oncul, S. Cikrikci, S. Taskiran, B. Tasan, S. Kaynak, F.B. Ozbey, A.P. Demchenko, Tetrahedron 63 (2007) 10290–10299.
[6] K.-i. Sakai, T. Tsuzuki, Y. Itoh, M. Ichikawa, Y. Taniguchi, Applied Physics Letters 86 (2005), 081103–081103-3;
F. Liang, L. Wang, D. Ma, X. Jing, F. Wang, Applied Physics Letters 81 (2002) 4–6;
J.E. Kwon, S.Y. Park, Advanced Materials 23 (2011) 3615–3642.
[7] S.J. Formosinho, L.G. Arnaut, Journal of Photochemistry and Photobiology A: Chemistry 75 (1993) 21–48;
S.M. Ormson, R.G. Brown, Progress in Reaction Kinetics 19 (1994) 45–91.
[8] H.-H.G. Tsai, H.-L.S. Sun, C.-J. Tan, Journal of Physical Chemistry A 114 (2010) 4065–4079.
[9] F. Rodríguez-Prieto, J.C. Penedo, M. Mosquera, Journal of the Chemical Society, Faraday Transactions 94 (1998) 2775–2782;
S.R. Vázquez, M.C.R. Rodríguez, M. Mosquera, F. Rodríguez-Prieto, Journal of Physical Chemistry A 112 (2008) 376–387.
[10] S.R. Vázquez, M.C.R. Rodríguez, M. Mosquera, F. Rodríguez-Prieto, Journal of Physical Chemistry A 111 (2007) 1814–1826.
[11] Q. Chu, D.A. Medvetz, Y. Pang, Chemistry of Materials 19 (2007) 6421–6429;
G. Yang, Z.A. Dreger, Y. Li, H.G. Drickamer, Journal of Physical Chemistry A 101 (1997) 7948–7952;
C.H. Kim, J. Park, J. Seo, S.Y. Park, T. Joo, Journal of Physical Chemistry A 114 (2010) 5618–5629.
[12] H. Wang, H. Zhang, O.K. Abou-Zied, C. Yu, F.E. Romesberg, M. Glasbeek, Chemical Physics Letters 367 (2003) 599–608.
[13] F.S. Rodembusch, L.F. Campo, V. Stefani, A. Rigacci, Journal of Materials Chemistry 15 (2005) 1537–1541;
J.J. Zheng, Y.X. Guo, X.P. Li, G.L. Zhang, W.J. Chen, Journal of Optics A: Pure and Applied Optics 68 (2006) 835–839;
R. Wang, D. Liu, K. Xu, J. Li, Journal of Photochemistry and Photobiology A: Chemistry 205 (2009) 61–69.
[14] Y. Wu, P.V. Lawson, M.M. Henary, K. Schmidt, J.-L. Bredas, C.J. Fahrni, Journal of Physical Chemistry A 111 (2007) 4584–4595;
J. Fahrni, M.M. Henary, D.G. VanDerveer, Journal of Physical Chemistry A 106 (2002) 7655–7663.
[15] M.M. Henary, Y. Wu, J. Cody, S. Sumalekshmy, J. Li, S. Mandal, C.J. Fahrni, Journal of Organic Chemistry 72 (2007) 4784–4797;
M.M. Henary, Y. Wu, C.J. Fahrni, Chemistry: A European Journal 10 (2004) 3015–3025.
[16] Y. Wu, X. Peng, J. Fan, S. Gao, M. Tian, J. Zhao, S. Sun, Journal of Organic Chemistry 72 (2007) 62–70.
[17] M.G. Holler, L.F. Campo, A. Brandelli, V. Stefani, Journal of Photochemistry and Photobiology A: Chemistry 149 (2002) 217–225;
F.S. Rodembusch, F.P. Leusin, L.F.d.C. Medina, A. Brandelli, V. Stefani, Photochemical & Photobiological Sciences 4 (2005) 254–259;
H.-J. Kim, J. Lee, T.-H. Kim, T.S. Lee, J. Kim, Advanced Materials 20 (2008) 1117–1121;
Y. Xu, Y. Pang, Chemical Communications 46 (2010) 4070–4072.
[18] F.-Y. Dupradeau, D.A. Case, C. Yu, R. Jimenez, F.E. Romesberg, Journal of the American Chemical Society 127 (2005) 15612–15617.
[19] A.S. Klymchenko, A.P. Demchenko, Journal of the American Chemical Society 124 (2002) 12372–12379;
D. LeGourriérec, V.A. Kharlanov, R.G. Brown, W. Rettig, Journal of Photochemistry and Photobiology A: Chemistry 130 (2000) 101–111;
T. Iijima, A. Momotake, Y. Shinohara, T. Sato, Y. Nishimura, T. Arai, Journal of Physical Chemistry A 114 (2010) 1603–1609.
[20] S. Park, O.-H. Kwon, S. Kim, S. Park, M.-G. Choi, M. Cha, S.Y. Park, D.-J. Jang, Journal of the American Chemical Society 127 (2005) 10070–10074.
[21] S. Park, J. Seo, S. Kim, S.Y. Park, Advanced Functional Materials 18 (2008) 726–731;
S. Park, J.E. Kwon, S.H. Kim, J. Seo, K. Chung, S.-Y. Park, D.-J. Jang, B.M. Medina, J. Gierschner, S.Y. Park, Journal of the American Chemical Society 131 (2009) 14043–14049.
[22] S. Kim, D.W. Chang, S.Y. Park, H. Kawai, T. Nagamura, Macromolecules 35 (2002) 2748–2753;
J.W. Chung, B.-K. An, S.Y. Park, Chemistry of Materials 20 (2008) 6750–6755.
[23] S. Kim, Q. Zheng, G.S. He, D.J. Bharali, H.E. Pudavar, A. Baev, P.N. Prasad, Advanced Functional Materials 16 (2006) 2317–2323.
[24] G.L. Silva, V. Ediz, D. Yaron, B.A. Armitage, Journal of the American Chemical Society 129 (2007) 5710–5718.
[25] S. Kim, T.Y. Ohulchanskyy, H.E. Pudavar, R.K. Pandey, P.N. Prasad, Journal of the American Chemical Society 129 (2007) 2669–2675;
Y. Li, F. Li, H. Zhang, Z. Xie, W. Xie, H. Xu, B. Li, F. Shen, L. Ye, M. Hanif, D. Ma, Y. Ma, Chemical Communications (2007) 231–233.
[26] J. Chen, B. Xu, X. Ouyang, B.Z. Tang, Y. Cao, Journal of Physical Chemistry A 108 (2004) 7522–7526;
H. Tong, Y. Hong, Y. Dong, M. Häussler, Z. Li, J.W.Y. Lam, Y. Dong, H.H.-Y. Sang, I.D. Williams, B.Z. Tang, Journal of Physical Chemistry B 111 (2007) 11817–11823.
[27] Z. Li, Y. Dong, B. Mi, Y. Tang, M. Häussler, H. Tong, Y. Dong, J.W.Y. Lam, Y. Ren, H.H.-Y. Sung, K.S. Wong, P. Gao, I.D. Williams, H.S. Kwok, B.Z. Tang, Journal of Physical Chemistry B 109 (2005) 10061–10066;
Y. Rean, J.W.Y. Lam, Y. Dong, B.Z. Tang, K.S. Wong, Journal of Physical Chemistry B 109 (2005) 1135–1140.
[28] H. Tong, Y. Hong, Y. Dong, Y. Ren, M. Häussler, J.W.Y. Lam, K.S. Wong, B.Z. Tang, Journal of Physical Chemistry B 111 (2007) 2000–2007;
X. Yang, Y. Zhou, T. Lei, N. Hu, E.-Q. Chen, J. Pei, Chemistry of Materials 22 (2010) 3735–3745.
[29] W.H. Melhuish, Journal of Physical Chemistry 65 (1961) 229–235.
[30] J.C. de Mello, H.F. Wittmann, R.H. Friend, Advanced Materials 9 (1997) 230–232.
[31] J. Pommerehne, H. Vestweber, W. Guss, R.E. Mahrt, H. Bassler, M. Porsch, J. Daub, Advanced Materials 7 (1995) 551–554.
[32] A.D. Becke, Journal of Chemical Physics 98 (1993) 5648–5652.
[33] J. Llano, J. Raber, L.A. Eriksson, Journal of Photochemistry and Photobiology A: Chemistry 154 (2003) 235–243.
[34] R. Bauernschmitt, R. Ahlrichs, F.H. Hennrich, M.M. Kappes, Journal of the American Chemical Society 120 (1998) 5052–5059.
[35] M.E. Casida, Journal of Chemical Physics 108 (1998) 4439–4449.
[36] R.E. Stratmann, G.E. Scuseria, M.J. Frisch, Journal of Chemical Physics 109 (1998) 8218–8224.

[37] J. Llano, L.A. Eriksson, Physical Chemistry Chemical Physics 6 (2004) 4707–4713.
[38] M.J.S. Dewar, E.G. Zoebisch, E.F. Healy, J.P.P. Stewart, Journal of the American Chemical Society 107 (1985) 3902–3909.
[39] G.B. Rocha, R.O. Freire, A.M. Simas, J.P.P. Stewart, Journal of Computational Chemistry 27 (2006) 1101–1111.
[40] G. Rauhut, T. Clark, T. Steinke, Journal of the American Chemical Society 115 (1993) 9174–9181.
[41] H. Mishra, S. Maheshwary, H.B. Tripathi, N. Sathyamurthy, Journal of Physical Chemistry A 109 (2005) 2746–2754.
[42] R. Misra, A. Mandal, M. Mukhopadhyay, D.K. Maity, S.P. Bhattacharyya, Journal of Physical Chemistry B 113 (2009) 10779–10791;
S. Mitra, R. Das, S.P. Bhattacharyya, S. Mukherjee, Journal of Physical Chemistry A 101 (1997) 293–298.
[43] A.R. Day, E.A. Steck, Journal of the American Chemical Society 65 (1943) 452–456.
[44] A.O. Eseaola, W. Li, R. Gao, M. Zhang, X. Hao, T. Liang, N.O. Obi-Egbedi, W.-H. Sun, Inorganic Chemistry 48 (2009) 9133–9146.
[45] A.O. Eseola, W. Li, W.-H. Sun, M. Zhang, L. Xiao, J.A.O. Woods, Dyes and Pigments 88 (2011) 262–273.
[46] J. Mahia, M. Maestro, M. Vazquez, M.R. Bermejo, A.M. Gonzalez, M. Maneiro, Acta Crystallographica Section C 55 (1999) 2158–2160.
[47] M. Swaminathan, S.K. Dogra, Journal of the Chemical Society-Perkin Transactions II (1983) 1641–1644.
[48] J. Hennesy, A.C. Testa, Journal of Physical Chemistry 76 (1972) 3362–3365.
[49] K.-C. Wu, P.-J. Ku, C.-S. Lin, H.-T. Shih, F.-I. Wu, M.-J. Huang, J.-J. Lin, I.-C. Chen, C.-H. Cheng, Advanced Functional Materials 18 (2008) 67–75.
[50] R. Kakker, V. Katoch, Journal of Molecular Structure: Theochem 578 (2002) 169–175.
[51] M.K. Nayak, B.H. Kim, J.E. Kwon, S. Park, J. Seo, J.W. Chung, S.Y. Park, Chemistry: A European Journal 16 (2010) 7437–7447.
[52] M. Sliwa, N. Mouton, C. Ruckebusch, S. Aloïse, O. Poizat, G. Buntinx, R. Métivier, K. Nakatani, H. Masuhara, T. Asahi, Journal of Physical Chemistry C 113 (2009) 11959–11968;
J.M. Ortiz-Sánchez, R. Gelabert, M. Moreno, J.M. Lluch, Journal of Chemical Physics 129 (2008) 214308–1214308.